THE AMERICAN MINERALOGIST

JOURNAL OF THE MINERALOGICAL SOCIETY OF AMERICA

Vol. 47 JULY-AUGUST, 1962 Nos. 7 and 8

CHLORITE POLYTYPISM: I. REGULAR AND SEMI-RANDOM ONE-LAYER STRUCTURES

B. E. BROWN AND S. W. BAILEY, *Department of Geology, University of Wisconsin, Madison, Wisconsin.*

ABSTRACT

Four different types of chlorite layers may be formed, taking due account of bonding restrictions, by the superimposition of "talc" and "brucite" sheets of ideal hexagonal geometry. Adjacent layers of the same type may be stacked in regular sequence to form 12 different 1-layer chlorite polytypes. The 12 ideal polytypes may be classified according to unit cell shape and symmetry with 2 structures based on an orthorhombic-shaped cell of monoclinic symmetry, 2 based on a triclinic cell with $\alpha=102°$ and $\beta=\gamma=90°$, and 8 based on a monoclinic-shaped cell with $\beta=97°$ and having monoclinic or triclinic symmetry. Single crystal x-ray study is required for complete differentiation of the regular-stacking polytypes, only three of which have been recognized to date. Most chlorites tend to have a fixed relationship between the talc and brucite sheets within each layer but a semi-random stacking sequence of adjacent layers wherein positions related by shifts of $\pm\frac{1}{3}b_0$ are adopted. Six ideal systems with semi-random stacking are possible, 2 based on an orthorhombic-shaped cell and 4 on a monoclinic-shaped cell, all distinguishable by powder photographs. Examination of powder photographs of chlorites from over 300 different localities has shown the existence of four of the six semi-random stacking types, the structures of which have been verified by additional study by single crystal methods. The relative abundances of the polytypes can be explained to a large extent by the amount of repulsion between the tetrahedral cations and the brucite cations and by the lengths of the interlayer hydrogen bonds in the structures. It is suggested that there is a tendency for the higher energy structures to form metastably in low energy environments, inverting to the most stable arrangement during metamorphism.

INTRODUCTION

The broad outlines of the chlorite structure were first recognized by Pauling (1930), and confirmed and refined by a number of later investigators. Two tetrahedral sheets of composition $OH(Si,Al)_2O_5$, one inverted relative to the other, are superimposed in such a manner that the opposing O+OH anion planes fit together in a somewhat expanded close-packed array, enclosing medium-sized cations such as Mg, Fe^{2+}, Fe^{3+}, Al, Cr, Ni, Mn, or Li in the octahedral interstices (Fig. 1a). Two negatively-charged talc-like sheets of this type are joined together by a positively-charged "brucite" sheet, nominally of composition $(Mg,Al)_3(OH)_6$ but with im-

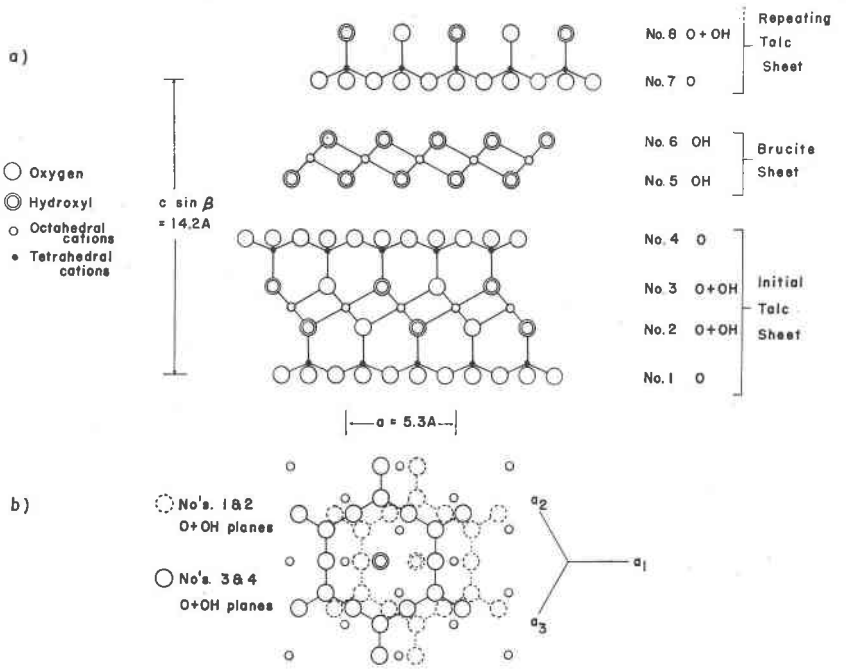

FIG. 1. Idealized chlorite structure (type II*b*). (a) 010 projection. The anion planes are numbered to facilitate discussion in the text of the possible stacking variations. (b) 001 projection of initial talc sheet, omitting tetrahedral cations. The arbitrary initial axes are not necessarily the same as those of the entire structure.

portant substitutions of Fe^{2+}, Fe^{3+}, Cr, Ni, Mn, or Li in certain varieties. The brucite sheet must be positioned in such a way that hydrogen bonds are formed between its two OH anion planes and the oxygen surfaces of the talc sheets above and below.

McMurchy (1934), Garrido (1949), and Brindley, Oughton, and Robinson (1950) have pointed out many of the details concerned with the superposition of adjacent sheets to form chlorite layers of different periodicities along the Z axis. They have been concerned mainly with finding structures to match the space groups observed for certain chlorites under study, rather than attempting to characterize all possible structures. Brindley, Oughton, and Robinson, in particular, have noted that in most chlorites adjacent layers are stacked with a considerable degree of randomness, as indicated by diffuse streaks along $k \neq 3n$ row- and layer-lines of x-ray rotation photographs. Chlorites having regular layer sequences appear to be less common, but are more amenable to detailed structure investigations.

The present study was begun as the first step in the determination of the crystal structure of a regular stacking 1-layer chromium-rich chlorite from Erzincan, Turkey (Brown and Bailey, 1960). It was evident that a knowledge of the unit cell parameters and symmetries of all theoretically possible 1-layer chlorites would facilitate the structure determination, as well as being of interest in the broader field of layer silicate polytypism. Accordingly a survey was undertaken of all permissible 1-layer assemblages, taking due account of the geometrical and bonding restrictions believed to be inherent in chlorite structures. Both regular and semi-random layer sequences were considered. The results of the theoretical considerations are presented in this paper in conjunction with a study of natural chlorites undertaken to determine the relative abundances of the theoretical polytypes that occur in nature, their compositional differences, and environmental significance. Subsequent papers in this series will describe the structures of several of the new polytypes in more detail.

Derivation of 1-Layer Polytypes

We are assuming at the outset of this study that the tetrahedral arrays form ideal undistorted hexagons and that no cation ordering takes place. The stacking of adjacent chlorite layers is assumed to be regular and the composition of all polytypes to be identical, namely that of clinochlore with 2 formula units of $(OH)_8Mg_5Al(Si_3Al)O_{10}$ in a base-centered cell. These assumptions are contrary in several respects to our knowledge of the detailed structures and compositions of chlorites. The consequences of these assumptions and the possible modifications needed to apply our results to natural chlorites are discussed in the following sections of this paper.

The different polytypes arise from the different permissible ways of superimposing the brucite sheet upon the "initial" talc sheet and the "repeating" talc sheet upon the brucite sheet. If we restrict the discussion to 1-layer chlorites, we need consider only one orientation of the initial talc sheet. This sheet will be oriented arbitrarily so that the $\frac{1}{3}a_0$ stagger between the two tetrahedral sheets at the octahedral close-packing junction is directed along the $-a_1$ axis of the initial talc sheet (Fig. 1b) and is pointing to the north in all the following diagrams (using map convention). The stagger could be directed equally well along the a_2 or a_3 axes of the initial talc sheet. These three arrangements, designated L, M, and N by Brindley, Oughton, and Robinson, are geometrically equivalent at this stage in the derivation since the axes of the entire assemblage have not been fixed.

All possible relations between the initial talc sheet, the brucite sheet, and the repeating talc sheet are expressible by translation or rotation of

the brucite and repeating talc sheets relative to a fixed initial talc sheet. The brucite sheet must superimpose upon the initial talc sheet so that hydrogen bonding is possible between the oxygens and the hydroxyls of the no. 4 and no. 5 anion planes of Fig. 1a. The geometry will be such as to allow the closest average approach of the no. 4 oxygens and the no. 5 hydroxyls.

Four different arrangements of the brucite sheet relative to the initial talc sheet prove to be possible. For convenience the brucite sheet will be designated I or II, as illustrated in Fig. 2a, according to occupancy of one or the other of the two alternate sets of octahedral cation sites. Brucite type I transforms to brucite type II by rotations of $\pm 60°$ or $180°$ of the entire sheet, and can be considered different only if described relative to the fixed initial talc sheet. A given brucite sheet, I or II, may be placed upon the initial talc sheet in two different positions, *a* or *b*. In position *a*, illustrated in Fig. 2b and 2d, one of the three brucite cations projects down onto the center of the hexagonal ring of oxygens in the uppermost talc anion plane and the other two cations project onto tetrahedral cations of this ring. In position *b*, illustrated in Fig. 2c and 2e, the brucite sheet is shifted by $\frac{1}{3}\ a_0$ so that the brucite cations form triads symmetrically disposed in projection to the hexagonal rings and tetrahedral cations below. It is convenient to designate these four structural arrangements I*a*, I*b*, II*a* and II*b*. They represent four different talc-brucite assemblages, which we shall refer to hereafter as chlorite layers.

The remaining considerations in the polytype derivation arise from articulation of the repeating talc sheet with the brucite portion of the chlorite layer below to achieve hydrogen bonding between the no. 6 hydroxyls and no. 7 oxygens (as numbered in Fig. 1a). The possible positions are best described in terms of shifts of the repeating talc sheet relative to the lower assemblage. If one superimposes the no. 8 O+OH anions on the no. 6 OH atoms of the brucite sheet (two anion planes below), then shifts of the upper talc sheet by $\pm\frac{1}{3}\ a_0$ along any of the three *a* axes of the lower assemblage give optimum hydrogen bond systems between the no. 6 and no. 7 anions. For each chlorite layer type, therefore, the hexagonal rings in the repeating talc sheet may be superimposed in six different orientations. These six orientations have been numbered arbitrarily, as in Fig. 3, according to the projected position of the no. 8 talc hydroxyl at the center of each hexagonal ring.

The position of the repeating talc sheet with respect to the position of the initial talc sheet is significant since the direction between equivalent points in the two sheets defines the Z axis of the resultant structure, and the distance between such equivalent points defines the *c* repeat. The orientation of this repeating talc sheet with respect to the stagger at its

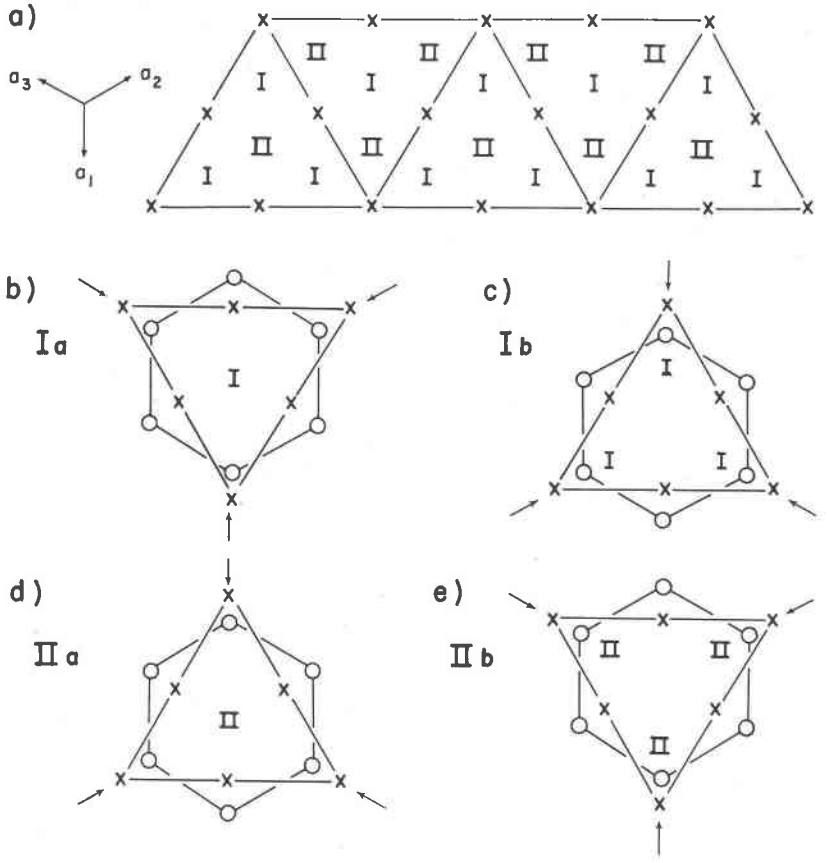

FIG. 2. Superimposition of brucite sheet upon initial talc sheet in 001 projection. (a) Brucite cations may occupy either sites I or II above no. 5 OH plane with no. 6 OH plane emplaced to provide octahedral coordination for the occupied sites. (b) and (c) Two methods (*a* and *b*) of positioning brucite sheet I upon initial talc sheet to provide hydrogen bonds between no. 4 O and no. 5 OH planes. The two resultant assemblages, designated I*a* and I*b*, are interrelated by shifts of the brucite sheet by $\frac{1}{3}\,a_0$ in the directions indicated by the small arrows. (d) and (e) Talc-brucite assemblages II*a* and II*b*.

octahedral interface must be identical with that of the initial talc sheet, inasmuch as 1-layer chlorites only are considered here. If a reference point is picked in the initial talc sheet, the projected vector between this point and the corresponding point in the repeating talc sheet illustrates the resultant shift between layers. The talc hydroxyls in the centers of the apical hexagonal rings in the no. 2 and no. 8 anion planes make convenient reference points. In Fig. 4 the arrow directed from OH no. 2 to OH no. 8 indicates the direction of the resultant interlayer shift and illustrates the relation between the initial and repeating talc sheets for 4 of the 6 possible positions of the repeating talc sheet upon the I*a* chlorite layer. Where the resultant interlayer shift is parallel to the direction of stagger between O+OH planes no. 2 and no. 3 at the octahedral junction of the initial talc

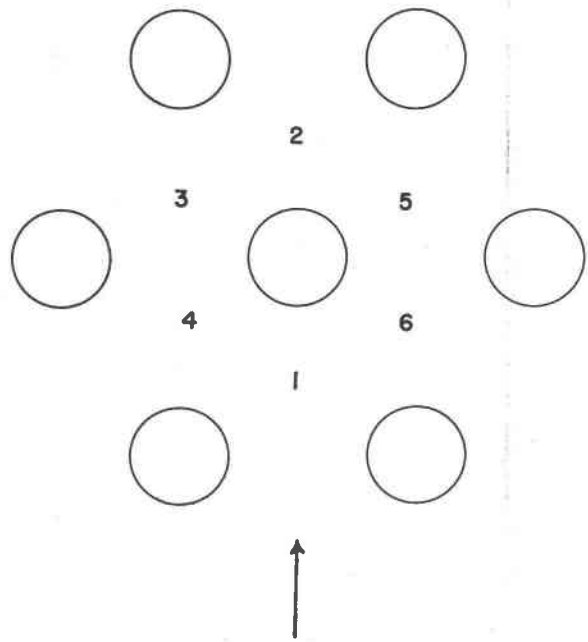

FIG. 3. Superimposition of repeating talc sheet on brucite sheet. Circles represent OH atoms in the upper plane of the brucite sheet, selected so as to form a hexagon centered on the mirror plane of the initial talc sheet. Hydrogen bonds from these hydroxyls to the basal oxygens of the repeating talc sheet result if a hexagonal ring (or no. 8 talc hydroxyl) in the overlying sheet projects onto one of the six numbered sites. The relationship of this section of the structure to the chlorite layer below is described in the text.

sheet (Figs. 4a,b), there is a mirror plane of symmetry and the ideal structures belong to the monoclinic space groups Cm or $C2/m$. Where the resultant interlayer shift is not parallel to the direction of octahedral stagger (Figs. 4c,d), the mirror plane is destroyed and the resultant symmetry is $C1$ or $C\bar{1}$.

Figure 3 and Table 1 may be used to summarize conveniently the results of the polytype derivation. The four chlorite layers, I*a*, I*b*, II*a*, and II*b*, can be specified in Fig. 3 by indicating the positions of the brucite cations and of the no. 2 and no. 3 initial talc hydroxyls relative to the diagram. Thus, brucite sheet I has its cations under sites, 2, 4, 6, and its no. 5 OH anions under sites 1, 3, 5, these positions being reversed for brucite sheet

TABLE 1. SUMMARY OF 1-LAYER POLYTYPES

Symbol	Space Group	Unique Angle	Equivalent Structure[2]	Enantiomorphic Structure[3]
I*a*-1	Cm	$\beta = 97°$	I*b*-2	—
I*a*-2[1]	$C2/m$	$\beta = 97°$	—	—
I*a*-3	$C1$	$\beta = 97°$	I*b*-6	I*a*-5
I*a*-4[1]	$C\bar{1}$	$\beta = 97°$	I*a*-6	—
I*a*-5	$C1$	$\beta = 97°$	I*b*-4	I*a*-3
I*a*-6	$C\bar{1}$	$\beta = 97°$	I*a*-4	—
I*b*-1[1]	$C2/m$	$\beta = 90°$	—	—
I*b*-2[1]	Cm	$\beta = 97°$	I*a*-1	—
I*b*-3[1]	$C\bar{1}$	$\alpha = 102°$	I*b*-5	—
I*b*-4[1]	$C1$	$\beta = 97°$	I*a*-5	I*b*-6
I*b*-5	$C\bar{1}$	$\alpha = 102°$	I*b*-3	—
I*b*-6	$C1$	$\beta = 97°$	I*a*-3	I*b*-4
II*a*-1[1]	$C2/m$	$\beta = 97°$	—	—
II*a*-2[1]	Cm	$\beta = 90°$	II*b*-1	—
II*a*-3[1]	$C\bar{1}$	$\beta = 97°$	II*a*-5	—
II*a*-4[1]	$C1$	$\alpha = 102°$	II*b*-5	II*a*-6
II*a*-5	$C\bar{1}$	$\beta = 97°$	II*a*-3	—
II*a*-6	$C1$	$\alpha = 102°$	II*b*-3	II*a*-4
II*b*-1	Cm	$\beta = 90°$	II*a*-2	—
II*b*-2[1]	$C2/m$	$\beta = 97°$	—	—
II*b*-3	$C1$	$\alpha = 102°$	II*a*-6	II*b*-5
II*b*-4[1]	$C\bar{1}$	$\beta = 97°$	II*b*-6	—
II*b*-5	$C1$	$\alpha = 102°$	II*a*-4	II*b*-3
II*b*-6	$C\bar{1}$	$\beta = 97°$	II*b*-4	—

[1] Selected among 12 unique polytypes.

[2] After 180° rotation about Y axis.

[3] Only one member of an enantiomorphic pair included in unique polytypes.

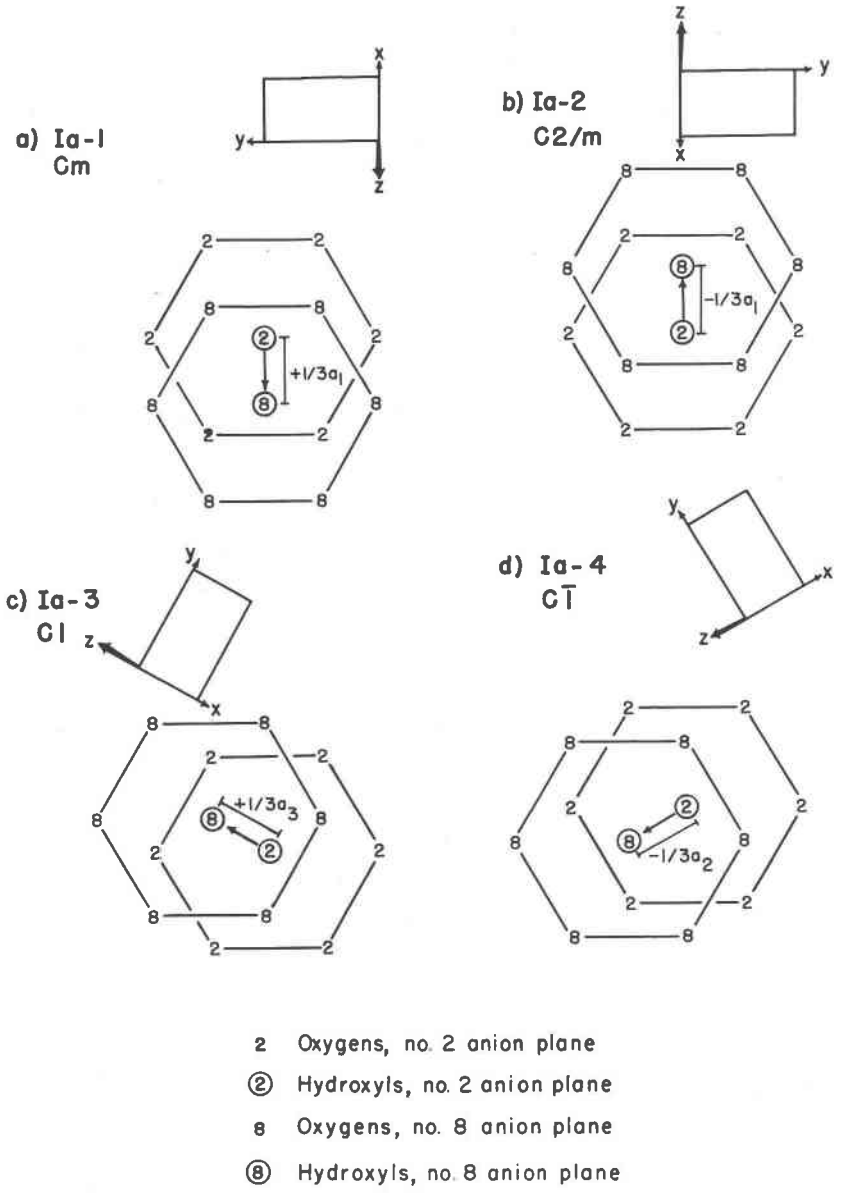

FIG. 4. Effect of interlayer shift direction in determining final symmetry for I*a* structures. The direction of octahedral stagger in both layers is along $-a_1$ of the initial talc sheet. The arrow directed from talc hydroxyl no. 2 to talc hydroxyl no. 8 indicates the direction of shift between the initial and repeating talc sheets. Cell axes for each polytype are illustrated, but interlayer shift directions are defined relative to arbitrary axes of initial talc sheet.

II. The no. 2 and no. 3 initial talc hydroxyls lie under sites 1, 2, or the central no. 6 hydroxyl of Fig. 3 as follows:

	I*a*	I*b*	II*a*	II*b*
no. 2 OH	central OH	site 1	site 2	site 1
no. 3 OH	site 2	central OH	site 1	central OH

The no. 8 talc hydroxyl may then superimpose upon any of the six numbered sites of the figure to give six polytypes for each of the four chlorite layers. The polytypes may be conveniently labeled I*a*-1 through I*a*-6, I*b*-1 through I*b*-6, and so forth. However only 12 of the resultant 24 structures prove to be significantly different from one another. Eight of the other structures are duplicates of some of these 12, exact equivalence being achieved by 180° rotation about the Y axis. Thus, the I*a*-odd structures are equivalent to the I*b*-even and the II*a*-even are equivalent to the II*b*-odd. An arbitrary choice has been made as to which structure of a duplicate pair shall be listed among the final 12 polytypes. There are also four pairs of enantiomorphic structures of symmetry *C*1 in the original 24 structures. Again because of equivalence relations only two enantiomorphic pairs prove to be different. Only one example from each different enantiomorphic pair has been included in the list of the 12 final structures, since the absolute configuration is difficult to determine in practice and is not of primary concern here. There are 14 different structures if the non-equivalent enantiomorphs I*b*-6 ($-$I*a*-3) and II*a*-6 ($=$II*b*-3) are included.

Table 1 lists the space groups, symbols, and equivalent structures for the 24 structures evolved in this study. Table 2 lists the atomic parameters for the 12 unique polytypes. The origin has been placed in the initial talc sheet on an octahedral position lying in the symmetry plane of the sheet. This origin lies in the symmetry plane of the chlorite structure, if one exists, and also coincides with a symmetry center for centrosymmetric structures.

Comparison with Previous Work

Of the 12 polytypes derived in this paper, only four appear to have been proposed as possible 1-layer structures by previous workers and only two have been verified by structural study of natural examples. McMurchy (1934) derived eight theoretical 1-layer structures of space group $C2/m$, as well as eight theoretical 2-layer structures of space group $C2/c$, in the first detailed structural study of chlorites. Unfortunately his work was done before the importance of the hydrogen bond was fully realized in restricting the position of the brucite sheet relative to the talc sheets above and below. As a result, five of his eight 1-layer structures do

TABLE 2. ATOMIC PARAMETERS OF 12 POLYTYPES

*C*2/*m* polytype	Atom	Mg_1	Mg_2	OH_1	O_1	Si_1	O_2	O_3	OH_2	OH_3	Mg_3	Mg_4
Ia-2	x/a	0	0	.357	.357	.397	.161	.411	.144	.144	0	0
	y/b	0	.333	0	.333	.333	.250	.500	0	.333	.167	.500
	z/c	0	0	.072	.072	.192	.233	.233	.433	.433	.500	.500
Ib-1	x/a	0	0	.333	.333	.333	.083	.333	.167	.167	0	0
	y/b	0	.333	0	.333	.333	.250	.500	.167	.500	0	.333
	z/c	0	0	.072	.072	.192	.233	.233	.433	.433	.500	.500
IIa-1	x/a	0	0	.357	.357	.397	.161	.411	.311	.311	0	0
	y/b	0	.333	0	.333	.333	.250	.500	.167	.500	.167	.500
	z/c	0	0	.072	.072	.192	.233	.233	.433	.433	.500	.500
IIb-2	x/a	0	0	.191	.191	.231	.245	.495	.144	.144	0	0
	y/b	0	.333	.500	.167	.167	0	.250	0	.333	.167	.500
	z/c	0	0	.072	.072	.192	.233	.233	.433	.433	.500	.500

$C\bar{1}$ polytype	Atom	Mg_1	Mg_2	OH_1	O_1	O_2	Si_1	Si_2	O_3	O_4	O_5	OH_2	OH_3	OH_4	Mg_3	Mg_4
Ia-4	x/a	0	0	.357	.357	.857	.397	.897	.161	.661	.911	.143	.143	.643	0	0
	y/b	0	.333	.333	0	.167	0	.167	.083	.083	.333	0	.333	.167	.167	.500
	z/c	0	0	.072	.072	.072	.192	.192	.233	.233	.233	.433	.433	.433	.500	.500
Ib-3	x/a	0	0	.167	.667	.667	.667	.667	.667	.417	.917	.333	.333	.833	0	0
	y/b	0	.333	.191	.024	.357	.064	.397	.245	.495	.495	.144	.477	.311	.167	.500
	z/c	0	0	.072	.072	.072	.192	.192	.233	.233	.233	.433	.433	.433	.500	.500
IIa-3	x/a	0	0	.357	.357	.857	.397	.897	.161	.661	.911	.311	.811	.811	0	0
	y/b	0	.333	.333	0	.167	0	.167	.083	.083	.333	.167	0	.333	.167	.500
	z/c	0	0	.072	.072	.072	.192	.192	.233	.233	.233	.433	.433	.433	.500	.500
IIb-4	x/a	0	0	.691	.191	.691	.231	.731	.245	.496	.995	.143	.143	.643	0	0
	y/b	0	.333	.333	.167	0	.167	0	.333	.083	.083	0	.333	.167	.167	.500
	z/c	0	0	.072	.072	.072	.192	.192	.233	.233	.233	.433	.433	.433	.500	.500

Cm polytype	Atom	Mg_1	Mg_2	OH_1	O_1	Si_1	O_2	O_3	OH_2	OH_3	Mg_3	Mg_4	OH_4	OH_5	O_4	O_5	Si_2	O_6	OH_6
Ib-2	x/a	0	0	.191	.191	.231	.245	.495	.477	.477	.167	.167	.356	.356	.005	.255	.269	.309	.309
	y/b	0	.333	.500	.167	.167	0	.250	0	.333	0	.333	.167	.500	.250	.500	.333	.333	0
	z/c	0	0	.072	.072	.192	.233	.233	.433	.433	.500	.500	.567	.567	.767	.767	.808	.928	.928
IIa-2	x/a	0	0	.333	.333	.333	.083	.333	.167	.167	.333	.333	0	0	.167	.417	.167	.167	.167
	y/b	0	.333	0	.333	.333	.250	.500	.167	.500	0	.333	0	.333	0	.250	.167	.167	.500
	z/c	0	0	.072	.072	.192	.233	.233	.433	.433	.500	.500	.567	.567	.767	.767	.808	.928	.928

*C*1 polytype	Atom	Mg_1	Mg_2	Mg_3	OH_1	O_1	O_2	Si_1	Si_2	O_3	O_4	O_5	OH_2	OH_3	OH_4	Mg_4	Mg_5	Mg_6	OH_5	OH_6	OH_7	O_6	O_7	O_8	Si_3	Si_4	O_9	O_{10}	OH_8
Ib-4	x/a	0	0	.500	.691	.191	.691	.231	.731	.245	.495	.995	.477	.477	.977	.167	.167	.667	.356	.856	.856	.255	.005	.505	.269	.269	.309	.309	.809
	y/b	0	.333	.167	.333	.167	0	.167	0	.333	.083	.083	0	.333	.167	0	.333	.167	.167	0	.333	.167	.417	.417	0	.333	0	.333	.167
	z/c	0	0	0	.072	.072	.072	.192	.192	.233	.233	.233	.433	.433	.433	.500	.500	.500	.567	.567	.567	.767	.767	.767	.808	.808	.928	.928	.928
IIa-4	x/a	0	0	.500	.167	.667	.667	.667	.667	.667	.417	.917	.333	.333	.833	.167	.167	.667	0	.500	.500	.083	.583	.833	.833	.833	.833	.833	.333
	y/b	0	.333	.167	.191	.024	.357	.064	.397	.245	.495	.495	.144	.477	.311	0	.333	.167	.189	.022	.356	.005	.005	.255	.103	.436	.143	.475	.309
	z/c	0	0	0	.072	.072	.072	.192	.192	.233	.233	.233	.433	.433	.433	.500	.500	.500	.567	.567	.567	.767	.767	.767	.808	.808	.928	.928	.928

not have optimum hydrogen bond arrangements. The other three structures correspond to our I*a*-2, II*a*-1, and II*b*-2 polytypes, with the exception that a different choice of origin is used. McMurchy believed that either the 1-layer II*b*-2 polytype or a 2-layer polytype (consisting of a II*b*-6 layer related to a II*b*-4 layer by a *c* glide plane) best fitted the *x*-ray data of the chlorites he had examined. Brindley *et al.* (1950) have pointed out however, that McMurchy was not justified in attempting to choose the exact structure involved, because he had used only the powder method of *x*-ray analysis and did not record any of the critical, but relatively weak, $k \neq 3n$ reflections. These reflections are requisite in determining any regular sequence of adjacent chlorite layers and degenerate to streaks for a random sequence. McMurchy's data was adequate, however, to justify his identification of the chlorite layer in his specimens as being the II*b* type.

Von Engelhardt (1942) also used the powder method in an attempt to work out the structure of a "chamosite" chlorite specimen having a unit cell of apparent orthorhombic shape but monoclinic symmetry. His results are suspect not only because of his use of powder data but also because of the fact that his proposed structure does not have an optimum hydrogen bond arrangement between the brucite and talc sheets, the hydroxyls and oxygens being exactly superimposed rather than slightly offset. A different structure will be proposed in this paper.

Garrido (1949) used single crystal methods to study a Cr-bearing chlorite having considerable randomness in the stacking of layers. He concluded that the brucite sheet maintains a fixed relationship to the talc sheet within a chlorite layer but that the repeating layer occupies at random three positions in which interlayer hydrogen bonds can be maintained. It should be noticed here that although we have recognized six positions of permissible articulation of the upper talc sheet, only three of these arrangements will give the $\beta = 97°$ angle observed for Garrido's specimen. Garrido's proposed structure, therefore, is a statistical average of our polytypes II*b*-2, II*b*-4, and II*b*-6. Because of the random stacking of layers observed for the specimen, the assignment of an exact 3-dimensional space group does not appear warranted. The space group $C2/m$ was assigned by Garrido on the basis of the *h*O*l* and O*k*O spectra. This represents only the symmetry of one chlorite layer, not of the entire crystal.

Robinson and Brindley (1949) and Brindley *et al.* (1950) have made the most extensive single crystal chlorite studies to date. They found examples of random, partly random, and regular stacking of layers within different crystals of a penninite sample. The crystals with regular layer sequences included two different 1-layer structures, one 2-layer, and one

3-layer structure. The two 1-layer structures proposed by these authors correspond to our II*b*-2 and II*b*-4 (or II*b*-6) polytypes, with a different choice of origin. The only major point of difference is their assignment of space group $C1$ to the II*b*-4 (or II*b*-6) polytype, their N (or M) structure. We have derived an ideal symmetry of $C\bar{1}$ for this structure on the basis of the assumptions of ideal hexagonal networks and no cation ordering. In an effort to resolve this difference we have applied the N(z) statistical test for a center of symmetry (Howells *et al.* (1950) to the intensity data listed for their crystal A. The effects of hypersymmetry arising from the repeat of many atoms in the structure at intervals of $\frac{1}{3}\ b_0$ and from the centrosymmetric nature of the individual talc and brucite sheets were avoided by using only $k \neq 3n$ reflections. The result is an acentric intensity distribution (Fig. 5*a*), confirming $C1$ as the actual space group. We have also obtained an acentric distribution (Fig. 5b) for the intensities listed for their L structure (our II*b*-2 polytype). This suggests a lower symmetry for the crystal than the $C2/m$ space group assigned by the authors and also determined as the *ideal* symmetry in our own derivation.

Steinfink (1958a,b; 1961) recognized and examined in more detail the same two polytypes from specimens of an oxidized prochlorite and a corundophyllite. The results of electron density maps and of bond length calculations suggest an ordered cation distribution, both tetrahedral and octahedral, in the monoclinic polytype II*b*-2 and a disordered distribution in the triclinic polytype II*b*-4. In both structures the ideal hexagonal networks are considerably distorted. Steinfink derived the structures using the space groups $C2$ and $C1$. These space groups appear to be correct on the basis of the acentric intensity distributions we have calculated from the published data (Figs. 5c,d).

Thus, the two natural polytypes that have been examined in some detail have symmetries lower than the ideal symmetries found in the present derivation, although there is no change in crystal system. This situation is not true for all natural chlorites, however, as illustrated in the Erzincan Cr-chlorite by coincidence of the observed space group $C\bar{1}$ with the ideal symmetry for the I*a*-4 polytype (Fig. 5e). Here also, as in Steinfink's monoclinic II*b*-2 polytype, electron density maps and bond length calculations suggest cation ordering as well as considerable distortion of the hexagonal networks (Brown and Bailey, 1960). Tetrahedral cation ordering within the plane of a single tetrahedral network would be impossible in certain of the structures without lowering the ideal symmetry. This is the case, for example, for all six monoclinic polytypes in the space groups $C2/m$ and Cm. Tetrahedral cation ordering is possible in the six triclinic polytypes of space groups $C\bar{1}$ and $C1$ without altering the ideal symmetry. Steinfink's triclinic II*b*-4 polytype, however, shows a

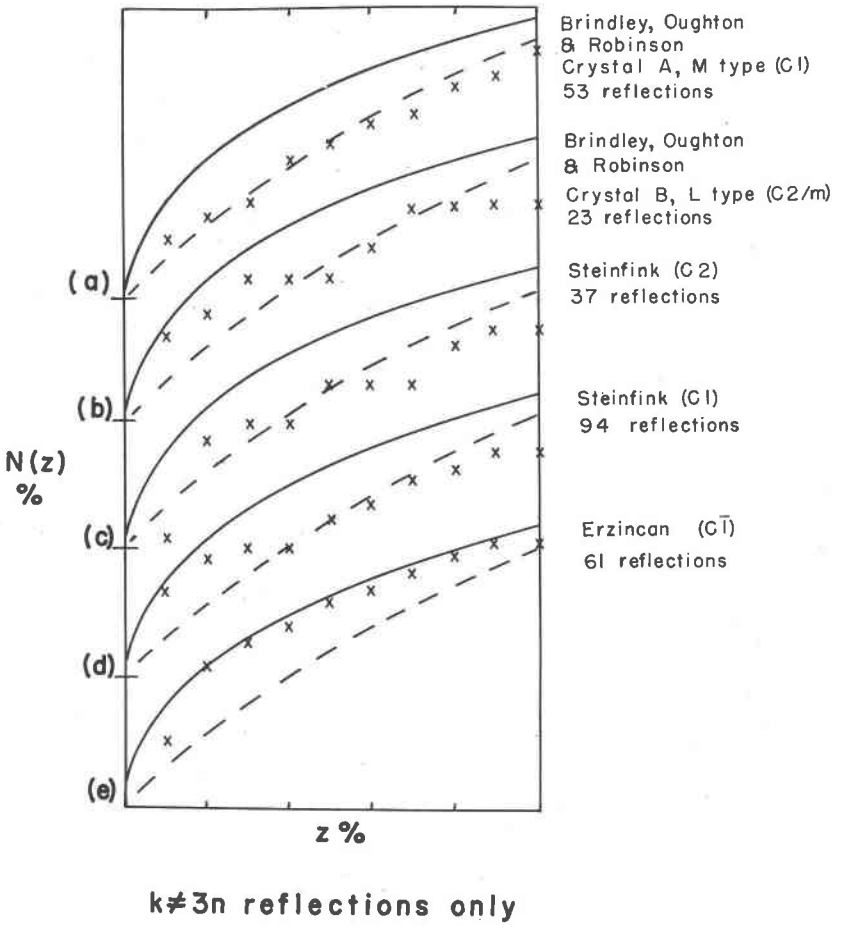

FIG. 5. N(z) statistical test for center of symmetry in five chlorite structures, using $k \neq 3n$ reflections to avoid hypersymmetry effects. The solid line indicates the theoretical intensity distribution for a centrosymmetric structure, dashed line the theoretical intensity distribution for a noncentrosymmetric structure. Individual curves are displaced vertically for clarity.

lower than ideal symmetry even though no ordering is present, indicating that ordering is only one of the factors that may be involved in reducing symmetry.

IDENTIFICATION OF POLYTYPES

The 12 theoretical regular-stacking polytypes may be differentiated by the comparison of observed with calculated x-ray intensities plus consideration of unit cell shape and symmetry. Three major groups of 1-

layer chlorites may be recognized on the basis of unit cell shape (not to be confused with symmetry)—(1) orthorhombic with $\alpha=\beta=\gamma=90°$, (2) triclinic with $\alpha=102°$ and $\beta=\gamma=90°$, and (3) monoclinic with $\beta=97°$.

The two polytypes that are based on an orthorhombic-shaped cell actually have monoclinic symmetry. I*b*-1 has an ideal symmetry $C2/m$ and II*a*-2 (equivalent to II*b*-1) has an ideal symmetry Cm. These structures have different (010) projections and, as a consequence, may be distinguished by their hOl intensities. Two polytypes, I*b*-3 and II*a*-4, (plus four equivalent and enantiomorphic structures) are based on a triclinic-shaped cell with $\alpha=102°$ and ideal symmetries of $C\bar{1}$ and $C1$ respectively. Alternatively, these two structures could be described either in terms of an orthorhombic-shaped 3-layer cell or a monoclinic-shaped cell with $\beta=102°$ and X and Y interchanged. Because of the triclinic symmetry there is no justification for adopting either of the latter cells. These triclinic polytypes have different (010) projections and, therefore, different hOl intensities. Powder photographs can be used to differentiate the I*b* and II*a* layer assemblages from one another since only the $2Ol$ reflections are required for this purpose. Powder photographs can not be used; however, to distinguish the orthorhombic-shaped cell from the triclinic-shaped cell for a particular layer assemblage, such as I*b*-1 from I*b*-3. These two structures differ only by a relative shift of the upper chlorite layer by $\frac{1}{3}b_0$. As a consequence, corresponding reflections of type $k=3n$ will have identical spacings and intensities for the two cells, although differing in l index. Single crystal data concerning either unit cell shape or symmetry, as recorded in $k\neq 3n$ reflections, are required for differentiation.

Identification of the eight polytypes having a monoclinic-shaped cell with $\beta=97°$ normally will require use of single crystal data also. The hOl intensities may be used to differentiate the four chlorite layers, I*a*, I*b*, II*a*, and II*b*, because these have different (010) projections. This part of the identification may be done either by single crystal or powder methods. The three polytypes resulting from different stacking positions of the repeating talc sheet upon a given chlorite layer, such as II*b*-2, II*b*-4, and II*b*-6, have identical (010) projections and hOl intensities. For each layer type only two of the three regular polytypes prove to be non-equivalent (neglecting enantiomorphic structures). Differentiation of these two polytypes from one another must be made on the basis of symmetry or hkl intensities, because of the identity of the hOl intensities.

It was mentioned in the last section that the symmetry of the natural chlorite may be lower than that of the idealized polytype. Thus, the observed space group for II*b*-2 is $C2$ rather than $C2/m$ and for II*b*-4 is $C1$ rather than $C\bar{1}$. In these examples the reduction is from a centrosymmetric to a non-centrosymmetric space group within a crystal system,

rather than a change in crystal system. This observation plus the adherence of the natural I*a*-4 polytype to the ideal symmetry $C\bar{1}$ suggests that the distinction between monoclinic and triclinic symmetry may be used in practice as an easy test to differentiate the two regular polytypes characteristic of each layer type and cell-shape. Nevertheless, only a few specimens have been studied in detail and we have not felt justified in using structural symbols, such as $1M_2$ or $1Tc_3$, to designate the theoretical polytypes of different systems. A complete nomenclature would require subscripts 1 through 6 for both the 1M types and the 1Tc types. Only 3 of the 12 regular-stacking polytypes have been recognized to date, and it seems likely in the future that most of the emphasis will be placed on recognizing the different chlorite polytypes that are possible with semi-random layer sequences.

We define semi-random layer sequences as those in which adjacent layers tend to adopt in irregular sequence only those permissable articulation positions that are related to one another by shifts of $\pm\frac{1}{3}\,b_0$. Using the numbering system of Fig. 3, this permits relative stacking sequences involving either positions 2, 4, and 6 or 1, 3, and 5, but not mixtures of the two sets. Each type of chlorite layer, therefore, may participate in two different semi-random stacking sequences. The eight resultant structures are reduced to six different polytypes by equivalence relationships (Table 1). Four of the six structures are based on a monoclinic-shaped cell with $\beta=97°$, one for each different layer type, and the other two structures are based on an orthorhombic-shaped cell. Each of the latter is really a statistical average of one orthorhombic-shaped cell and two triclinic-shaped cells with $\alpha=102°$, but these three cells become indistinguishable with semi-random stacking because of the degeneracy of $k\neq 3n$ reflections. In this series of papers the cell will be described as orthohexagonal in cases where the true shape and symmetry can not be determined, either because of semi-random layer stacking or the lack of single crystal data. The symmetry of all the semi-random stacking sequences is triclinic, being a statistical average of one monoclinic and two triclinic arrangements. This average symmetry is not determinable because of the loss of true periodicity along Z for those atoms that are not spaced at intervals of $\frac{1}{3}\,b_0$ within each layer. This results in streaking of $k\neq 3n$ reflections along c^*. The sharp $k=3n$ reflections give the symmetry of the individual layers, always monoclinic for the ideal configurations.

Table 3 contains hOl structure amplitude data for the I*a*, I*b*, II*a*, and II*b* assemblages of different cell shapes, as computed from the ideal coordinates listed in Table 2. The values listed are valid both for regular and semi-random layer sequences. We have not thought it worthwhile to include $k\neq 3n$ structure amplitudes for the individual regular-stacking

polytypes, because of their apparent infrequent occurrence. Symmetry and cell-shape considerations are sufficient to identify a regular-stacking polytype once the layer type is determined from the *hOl* intensities. All six semi-random stacking chlorite types can be identified conveniently by powder photographs, using the data of Table 3. In particular, chlorites based on the orthorhombic-shaped cell have a pattern geometry considerably different from that of chlorites based on a monoclinic-shaped cell.

Because all layer silicates analyzed structurally to date have contained distorted hexagonal networks, some deviations of the observed structure amplitudes from those calculated from idealized coordinates are to be expected. Examples are given in Table 3 of the actual single crystal structure amplitudes measured for the I*a*-4 and II*b*-4 structures so that an idea can be obtained of the deviations to be expected. The values in Table 3 were computed primarily for comparison with observed structure amplitudes in single crystal study. In attempting to compare the calculated structure amplitudes with intensities observed on powder patterns, variations that may arise from crystal perfection, multiplicity, *x*-ray dispersion, and the Lorentz-polarization factor must be considered in addition to any structural variations due to network distortion, cation ordering, and isomorphous substitution. We have found, nevertheless, that there is quite a close correlation with powder pattern intensities, provided one takes into account the increased intensities of the first few *hOl* reflections due to the large effect of the Lorenz-polarization factor at low θ values. The deviations from the ideal values are not great enough to prevent identification of the polytypes.

Survey of Natural Chlorite Polytypes

There has been a tendency among mineralogists in recent years to assume that all chlorite minerals are based on the same structural arrangement. This tendency probably results from the structure determinations of McMurchy (1934), Garrido (1949), Brindley *et al.* (1950), and Steinfink (1958a,b; 1961). In all of these structures the layers have been found to be of the same type, the II*b* assemblage. The polytypism observed has been a result of variation in the manner of stacking of adjacent layers of the same sort. The powder patterns available in the literature also indicate that the II*b* assemblage is the common chlorite structural scheme. The work of von Engelhardt (1942) and of Shirozu (1955, 1958a, 1960a), however, proves the existence of an orthohexagonal chlorite as well. It will be shown in this section that approximately 80 per cent of all chlorites have the II*b* structure, but that at least three other structures exist. There appears to be sufficient environmental and compositional significance attached to the other structures that have been identified to war-

TABLE 3. *h0l* STRUCTURE AMPLITUDES OF POLYTYPES[1]

$\beta=97°$ Polytypes								$\beta=90°$ Polytypes			
		F_{calc}				F_{obs}				F_{calc}	
d(Å)	*h0l*	I*a*	I*b*	II*a*	II*b*	I*a*	II*b*	d(Å)	*h0l*	I*b*	II*a*
2.66	$20\bar{1}$	44	41	60	7	43	28	2.67	200	8	25
2.65	200	86	52	52	15	106	0		201	32	78
2.59	$20\bar{2}$	68	91	6	96	69	98	2.62	$20\bar{1}$	58	55
2.55	201	58	58	134	117	34	137		202	208	142
2.44	$20\bar{3}$	1	192	96	151	23	133	2.50	$20\bar{2}$	49	97
2 39	202	218	20	117	98	199	94		203	22	112
2.26	$20\bar{4}$	44	99	151	89	62	94	2.33	$20\bar{3}$	44	115
2.20	203	26	61	80	39	29	23		204	164	57
2.07	$20\bar{5}$	53	135	46	38	55	49	2.13	$20\bar{4}$	68	93
2.01	204	147	41	55	153	152	142		205	58	58
1.88	$20\bar{6}$	38	89	112	87	53	92	1.95	$20\bar{5}$	7	121
1.83	205	19	32	44	104	28	82		206	194	88
1.72	$20\bar{7}$	60	182	100	73	74	41	1.77	$20\bar{6}$	28	102
1.67	206	217	54	189	84	161	55		207	62	176
1.57	$20\bar{8}$	120	111	124	194	120	134	1.62	$20\bar{7}$	35	91
1.52	207	46	136	39	27	27	32		208	134	75
1.435	$20\bar{9}$	65	78	91	32	53	24	1.478	$20\bar{8}$	190	102
1.398	208	47	131	82	192	47	130		209	60	68
1.335	$40\bar{1}$	81	36	91	4	63	0	1.358	$20\bar{9}$	71	169
1.332	$40\bar{2}$	94	93	76	57	89	31	1.335	400	10	42
1.325	400	66	119	30	138	42	102		401	96	78
1.320	$2, 0, \bar{1}0$	209	67	162	30	171	32	1.329	$40\bar{1}$	71	110
1.318	403	98	40	141	85	60	59		402	1	51
1.305	401	38	147	17	111	15	79	1.312	$40\bar{2}$	185	135
1.294	$40\bar{4}$	137	70	79	129	115	85		403	87	132
1.288	209	79	160	131	84	62	48	1.285	$40\bar{3}$	20	43
1.275	402	94	61	157	15	85	23		2, 0, 10	33	110
1.261	$40\bar{5}$	75	82	12	11	57	0	1.254	$2, 0, \bar{1}0$	150	69
1.237	403	14	72	46	13	0	0		404	63	64
1.221	$40\bar{6}$	91	17	35	68	78	51	1.250	$40\bar{4}$	59	17
1.195	404	13	73	33	101	0	68		405	45	62
1.192	2, 0, 10	4	62	54	14	0	0	1.208	$40\bar{5}$	23	60

[1] Calculated for clinochlore composition, assuming ideal hexagonal nets and no cation ordering, with $a=5.34$ Å, $c \sin \beta=14.20$ Å. F_{obs} for the I*a* and II*b* structures taken from Brown and Bailey (1960) and Steinfink (1958b) respectively.

rant their recognition and study by mineralogists and petrologists.

We have attempted to determine the relative abundances of the polytypes by examining reliable data for chlorites from 303 different localities, 67 patterns taken from the literature and 236 patterns prepared either

from specimens in the University of Wisconsin collections or acquired through loan and donation. Four of the six chlorite types recognizable by the powder method have been identified. These include 243 examples of the II*b* assemblage, 37 examples of the I*b* assemblage based either on the orthorhombic- or triclinic-shaped cell, 13 examples of the I*b* assemblage based on a monoclinic-shaped cell, and 10 examples of the I*a* assemblage. It has been possible to study at least one specimen of each of these four structural types by single crystal methods and thereby to verify the powder pattern indexing and the calculated structure amplitudes listed in Table 3 for these assemblages.

Von Engelhardt (1942) and Shirozu (1955, 1958a), have published powder data for five chlorite specimens that they have indexed on the basis of an orthorhombic-shaped cell. It is not certain whether these are regular or semi-random stacking polytypes, since no unambiguous $k \neq 3n$ reflections are recorded. Shirozu (1960a) also lists the chemical compositions of 12 additional Japanese orthohexagonal chlorites for which the powder patterns, although not published, are stated to be similar. Twenty specimens from the University of Wisconsin collections give patterns very similar to those of von Engelhardt and Shirozu. All appear to have the I*b* structure on the basis of the powder pattern evidence. Because the symmetry of the orthohexagonal I*b* assemblage with regular layer sequencies may be either monoclinic or triclinic, but not orthorhombic, $h0l$ and $h0\bar{l}$ reflections will have identical d values but different intensities. *X*-ray powder data, because of superposition of these reflections, give the combined values of $F^2(h0l)+F^2(h0\bar{l})$. The individual intensities can be verified only by single crystal data. Dr. Shirozu of Kyushu University kindly supplied us with suitable single crystals from hydrothermal quartz-copper veins in the Sayama mine and the Arakawa mine of Japan. Miss Judy Smith of this laboratory has examined approximately 100 individual crystals from these two samples by precession and oscillation techniques. The results confirm the structure amplitudes of the I*b* assemblage listed in Table 3. No examples of regular layer sequences were found. We suggest that the I*b* structure is more plausible than that deduced by von Engelhardt, because of the more favorable hydrogen bond arrangement, and that it gives better agreement between the calculated and observed $h0l$ structure amplitudes.

Identification of the I*b* orthohexagonal chlorite must be made with caution in the case of mixtures. The pattern is very similar, with the major exception of the 14 Å line, to that of the hexagonal form of "chamosite" (7 Å berthierine) described by Brindley (1951). *X*-ray data may not be definitive without heating and chemical treatments for mixtures of a chlorite with 7 Å chamosite or serpentine. For this reason two apparent

mixtures of this type described by Shirozu (1958a,b) have not been included here as proved examples of the I*b* orthohexagonal chlorite. Another possible identification difficulty lies in the similarity of the lines in the orthohexagonal I*b* pattern to the more intense lines in the powder pattern given by the monoclinic-cell I*b* assemblage. Although the weaker lines in the latter pattern will identify the cell shape and will serve to differentiate the two chlorite types, these lines tend to disappear in the less well-crystallized varieties. The patterns then differ only by a spacing variation in the observable $20l$ lines of about 0.05 Å for the ideal compositions, a difference that might be partly or wholly compensated for by compositional variation and by distortion of the ideal cell shape. Careful indexing on the basis of both cells is advisable if the lines tend to be diffuse and the spacings intermediate between the ideal values given in Table 3 for the orthorhombic- and monoclinic-shaped cells.

The I*b* structure with a monoclinic-shaped cell has been identified in 13 specimens from the Wisconsin collections. All 13 powder patterns are diffuse with the weaker hOl and $hO\bar{l}$ reflections merging into the film background. Most of the patterns can be indexed only by assuming β values slightly larger than the ideal value of 97°, the observed values ranging between 97° and 98°. A lower tetrahedral-Al content than for other structural types is suggested by the higher basal spacings. Single crystal precession photographs, which verify the powder pattern indexing and the intensities calculated for the monoclinic-cell I*b* structure, were obtained for a specimen of diabantite occurring as vesicle fillings in Triassic trap rocks at New Britain, Connecticut.

The I*a* assemblage has been recognized in three Fe-rich, one Cr-rich, and six Li-rich specimens. It is also the structural scheme commonly adopted by vermiculite. The Cr-rich chlorite from Erzincan, Turkey, is especially well crystallized, showing a variety of crystal faces in addition to the basal pinacoid. We have examined over 40 single crystals from this specimen. The structural scheme is based on the I*a* assemblage with $\beta = 97°$ and is recognizable in crystals having semi-random or regular stacking of layers. Several multi-layer polytypes have been recognized, but the 1-layer I*a*-4 structure is predominant. A powder pattern of similar material from Erzincan published by Lapham (1958) is recognizable as distinctly different from those of the other Cr-chlorites of his study, which are based on the II*b* assemblage. The detailed structure of a regular-stacking, 1-layer I*a*-4 crystal from Erzincan will be reported in the second paper of this series.

The six Li-rich cookeites examined give nearly identical powder patterns. Single crystal photographs have been obtained for four of these specimens but no examples of regular stacking have been found. Bram-

mall, Leech, and Bannister (1937) have determined the ideal composition of cookeite to be $(LiAl_4)(Si_3Al)O_{10}(OH)_8$. Norrish (personal communication) has computed a 1-dimensional electron density projection that suggests the "talc" sheet is dioctahedral ($Al_{1.78}Li_{0.36}$) whereas the "brucite" sheet is trioctahedral ($LiAl_2$). Our single crystal intensity data agree quite closely with the data calculated for the ideal I*a* structure despite the differences in the numbers and scattering powers of the octahedral cations. A somewhat similar "dioctahedral" chlorite believed to have mixed dioctahedral and trioctahedral sheets (Bailey and Tyler, 1960) has $20l$ intensities that fit those calculated for the II*b* structure.

During our study of chlorites we have obtained powder patterns for a number of vermiculite specimens, for all of which the I*a* structure is suggested on the basis of the $20l$ intensities. The structure of a 2-layer vermiculite determined by Mathieson and Walker (1954) and by Mathieson (1958) corresponds to a somewhat irregular alternation of I*a*-4 and I*a*-6 layers with incomplete occupancy of the brucite atomic positions by Mg and H_2O.

No examples of either the orthohexagonal- or monoclinic-cell II*a* structures have been recognized. Both present identification difficulties. The pattern of the orthohexagonal II*a* chlorite, with the exception of the diagnostic 14 Å line, is similar to that of 7 Å amesite and of certain aluminous serpentines (Gillery, 1959; Bailey and Tyler, 1960). The pattern of the monoclinic-cell II*a* chlorite has $20l$ and $20\bar{l}$ intensities sufficiently similar to those of the common II*b* chlorite to require considerable caution in identification.

Almost all the chlorite specimens examined could be classified by means of powder patterns into either the orthohexagonal-cell I*b* or monoclinic-cell I*a*, I*b*, or II*b* categories. This immediately implies that the brucite sheet maintains a fixed position relative to one adjacent talc sheet, either above or below, verifying the existence of at least three different types of chlorite layers. The observance of sharp $k=3n$ and of streaked $k\neq 3n$ reflections on most of the single crystal photographs indicates that the layer sequences are semi-random rather than completely random. Only those articulation positions that preserve the same unit cell shape tend to be adopted by adjacent layers. If this were not true, it would not be possible to classify chlorites into one or another of the observed layer types. Complete disappearance of the $20l$ reflections, observed for only four specimens of this study, results from more drastic disorder. Two structural interpretations seem possible for this type of pattern. Adjacent layers may adopt randomly all six articulation positions that permit hydrogen bonds between layers. Alternatively, the brucite sheet may be positioned semi-randomly relative to both adjacent talc sheets, thus

maintaining hydrogen bonds but eliminating unique layer types. Approximately 10 per cent of the patterns examined in this study show well defined but weak $02l$ and $11l$ lines characteristic of regular layer sequences. Since these $k \neq 3n$ reflections are difficult to observe and may be destroyed by specimen grinding, it is probable that the ratio of regular to semi-random stacking polytypes is actually somewhat greater than 10 per cent.

Representative powder photographs are tabulated in Table 4. These patterns may be compared with the ideal spacings and structure amplitudes of Table 3. Octahedral Li and Al decrease the hOl spacings relative to the ideal values whereas octahedral Fe increases the spacings. The most noticeable discrepancy in the observed and calculated intensities is the reversal of the relative importances of the $20\bar{2}$ and 201 intensities in

TABLE 4. REPRESENTATIVE POWDER PATTERNS[1]

1			2		3		4			5		
hkl	*d*(Å)	I	d(Å)	I	d(Å)	I	*hkl*	d(Å)	I	*hkl*	d(Å)	I
001	14.15	8	14.4	6	14.2	6	001	14.1	8	001	14.2	6
002	7.05	10	7.15	10	7.10	10	002	7.05	7	002	7.10	9
003	4.72	6	4.79	4	4.73	4	003	4.70	9	003	4.75	2½
02; 11	4.60	2	4.63	4	4.63	1	02; 11	4.47	4	02; 11	4.62	3½
004	3.54	10	3.59	7	3.55	8	004	3.52	9	004	3.56	7
005	2.83	4	2.87	2½	2.84	3	005	2.815	3	005	2.85	2
$20\bar{1}$	2.66	1½	2.68	4	—		200	2.56	4	200	2.685	2
200	—		—		2.66	4	$20\bar{2}$	2.505	7	201	2.64	1½
$20\bar{2}$	2.59	5	2.61	1½	2.59	½	201	2.465	½	202	2.505	10
201	2.54	8	2.55	½	2.55	1	$20\bar{3}$	2.37	½	203	2.33	1
$20\bar{3}$	2.44	7	2.475	6	—		006	2.35	½	204	2.14	4
202	2.38	4	2.39	1	2.395	6	202	2.315	10	007	2.03	½
$20\bar{4}$	2.255	4	2.29	1	2.27	1	$20\bar{4}$	2.205	1	205	1.955	½
203	—		2.20	½	—		203	2.14	½	206	1.78	3
$20\bar{5}$	2.06	1½	2.105	2	2.07	½	$20\bar{5}$	2.015	3	008		
007	—		2.045	½	—		007			15; 24; 31	1.75	1
204	2.00	6	2.01	1	2.01	3	204	1.96	5	207	1.62	½
$20\bar{6}$	1.88	2½	1.91	½	1.89	½	$20\bar{6}$	1.845	½	060	1.548	6
205	1.82	2½	—		—		008	1.76	1	062	1.515	2½
15; 24; 31	1.74	1	1.758	2	1.76	½	15; 24; 31	1.685	3	208	1.482	2
207	1.715	½	1.74	1	—		$20\bar{7}$			064	1.422	2
206	1.66	1½	—		1.67	2½	206	1.635	4½	0, 0, 10		
$20\bar{8}$	1.565	3	—		1.57	1	$20\bar{8}$	1.54	2½	065	1.360	1
060	1.538	7	1.548	6	1.549	6	060	1.489	7	209		
062	1.503	2½	1.515	3	1.515	3	062	1.458	1½			
063	1.462	½	1.478	1	1.472	1	$20\bar{9}$	1.420	1½			
$20\bar{9}$	—		—		1.439	½	063					
0, 0, 10	1.414	1	1.434	½	1.420	3	0, 0, 10	1.410	1½			
064			1.420	1			064	1.372	1½			
208	1.392	2½	—		—		208					

[1] 114.6 mm diameter camera, Fe Kα radiation, spacings corrected for shrinkage, intenstities estimated visually. The indices in Col. 1 apply to the patterns in Col. 1–3.

1. II*b* chlorite, Buck Creek, North Carolina. 2. I*b* chlorite (monoclinic cell), New Britain, Connecticut. 3. I*a* chlorite, Vicar mine, Michigan. 4. I*a* cookeite, Londonderry, Western Australia. 5. I*b* chlorite (orthohexagonal cell), Florence mine, Wisconsin.

the Fe-bearing I*a* chlorites, illustrated in Table 4 by the Vicar mine specimen. This effect can be shown by structure factor calculation to be due to concentration of Fe in the talc sheet.

Polytype Stabilities

The relative abundances of the polytypes can be explained to a large extent on the basis of two structural features. The different talc-brucite-talc sequences provide varying amounts of cation superposition and, thereby, cation repulsion. Superposition of octahedral and tetrahedral cations within the talc sheet is precluded by the geometry of the sheet. Superposition may occur between cations of adjacent talc and brucite sheets or between cations of the initial and repeating talc sheets, depending on the relative positions of the sheets. The observed abundances of the polytypes decrease with increasing repulsion between the brucite cations and the tetrahedral cations above or below. Repulsion between cations separated by one-half the chlorite layer thickness or more does not seem to be effective in influencing the abundances. The relative lengths of the hydrogen bonds from the brucite sheet to the two opposing talc oxygen surfaces, determined primarily by the direction and amount of distortion of the ideal hexagonal talc networks, provide a second influence. The relative bond lengths appear to account for important modifications of the order of abundance predicted on the basis of cation repulsion alone. In the chart below a rating of 1 is given for minimum cation repulsion and for minimum hydrogen bond length, a rating of 2 for intermediate values, and a rating of 3 for maximum values.

Polytype	Cation Repulsion	Hydrogen Bond	Number of Specimens Observed
II*b*, $\beta=97°$	1	1	243
I*b*, $\beta=90°$	1	3	37
I*b*, $\beta=97°$	2	2	13
II*a*, $\beta=90°$	2	2	0
I*a*, $\beta=97°$	3	1	10
II*a*, $\beta=97°$	3	3	0

The great abundance of the II*b* chlorites is evidently due to the very favorable combination of minimum cation repulsion with minimum hydrogen bond length. The orthohexagonal I*b* chlorite, which also has a minimum amount of cation repulsion, is the second most abundant variety. Its stability is decreased markedly by a relatively unfavorable, high energy interlayer bond arrangement. The main discrepancy in the chart is that it predicts that the monoclinic-cell I*b* and orthohexagonal-cell II*a* chlorites should be equally abundant. It is not possible at this stage to judge whether our failure to observe any orthohexagonal II*a*

chlorites is due to bias in our selection of samples or to some other factor that affects the II*a* structure adversely. The absence of the monoclinic-cell II*a* chlorite, on the other hand, is understandable from the unfavorable chart ratings indicating both a maximum amount of cation repulsion and maximum hydrogen bond lengths. The I*a* structure also has a maximum amount of cation repulsion but this adverse factor is reduced somewhat by the low energy interlayer bond system. In the Erzincan I*a* chlorite an effective distribution of charges is achieved by cation ordering such that the highest charged brucite cation, Cr^{3+}, is positioned exactly between the tetrahedral sites of lowest charge, Al^{3+}, in the talc sheets above and below. The stability of the I*a* structure is enhanced further in vermiculite by the mechanism of a reduced interlayer cation population, lowering the total amount of cation repulsion.

Although the chart explains the broad features of the observed abundance pattern quite well, some uncertainties are involved in the ratings used for hydrogen bond lengths. The detailed distortions of the ideal hexagonal networks and the resultant hydrogen bond lengths are not known for the I*b* and II*a* structures. It has been necessary to assume that the direction of rotation of tetrahedra relative to the octahedral cations is the same as that found in the I*a* and II*b* chlorite structures. This assumption seems reasonably valid because the rotation is in the same direction for dickite (Newnham, 1961), muscovite (Radoslovich, 1960), and vermiculite (Mathieson and Walker, 1954) as well, only that of amesite (Steinfink and Brunton, 1956) being in the opposite sense.

Composition undoubtedly influences the stability of chlorite polytypes through its effect on the cation charges and on the amount of distortion of the hexagonal networks. Although we have not attempted to determine chemical compositions directly, we do have some indirect information in the form of unit cell dimensions. Shirozu (1960a) has used calibrated *x*-ray spacing graphs to determine the compositions of 46 Japanese monoclinic chlorites, presumably having the II*b* structure. His results plus those for 65 of our own II*b* specimens are shown in Fig. 6a. We have used Shirozu's composition graphs (1958a, 1960b), which assume a low concentration of trivalent ions other than Al, to assure a valid comparison of the two sets of data. We believe that the measurement of chlorite compositions by this method, although not absolute, will serve to show up significant differences in the compositional fields of the polytypes. We have not entered our own results in areas of the diagram where Shirozu's data are already adequate, and have attempted only to outline the boundaries of the II*b* compositional field so far as possible from the data at hand. Figure 6b illustrates the compositions of all the other structural types encountered in this study, exclusive of the cookeites,

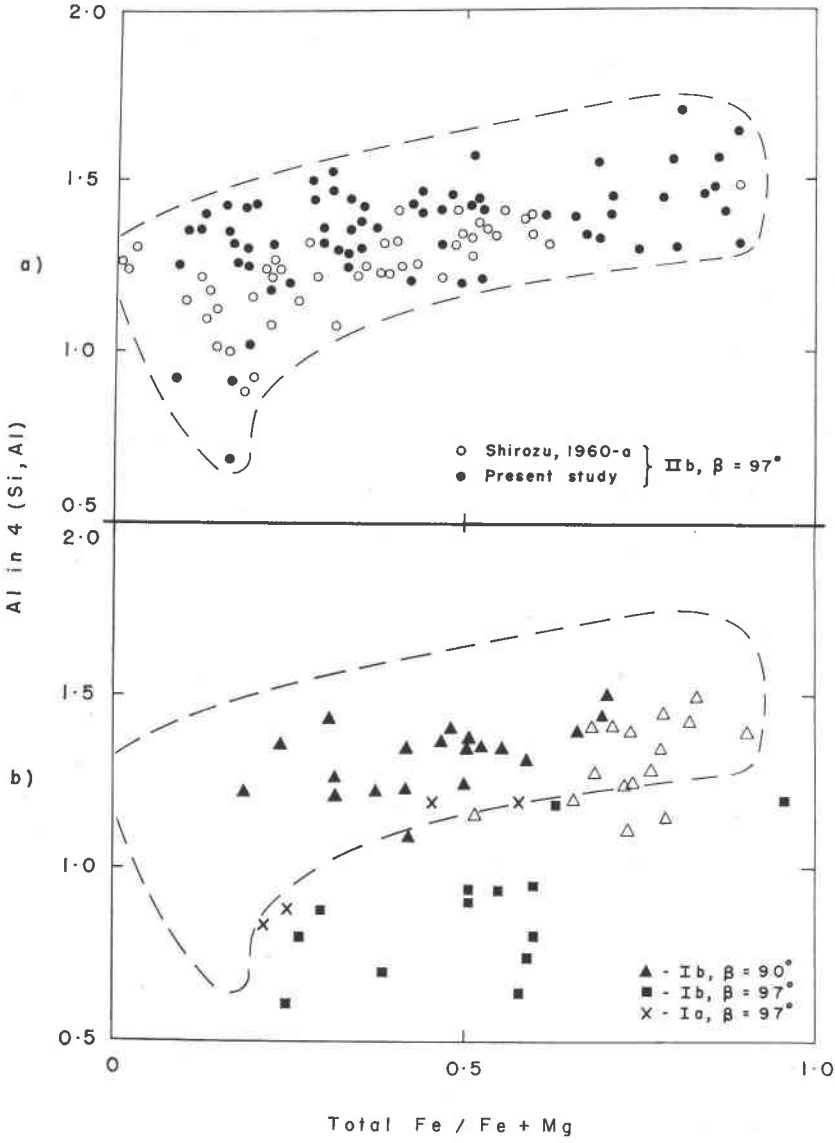

FIG. 6. (a) Tentative composition field of II*b* chlorites, as determined from *x*-ray spacing graphs. (b) Compositions of other chlorite polytypes. Open triangles represent data of Shirozu (1960a) for hydrothermal orthohexagonal 1*b* chlorites from Japan.

relative to the compositional field of the II*b* structure. Comparison of Figs. 6a and 6b shows that there is considerable overlap of the composition fields of the II*b* and the orthohexagonal I*b* chlorites. The II*b* types are somewhat more abundant at high Mg compositions and the I*b* types at high Fe compositions, especially for Shirozu's specimens.

There is a definite trend for increasing tetrahedral Al substitution to be accompanied by a corresponding increase in octahedral Fe. Shirozu (1960a) has noted this same trend for his specimens and has attributed it to the need for maintaining a certain degree of fit between the tetrahedral and octahedral sheets. The structural types cut across most of the arbitrary nomenclature divisions that have been established for chlorite varieties of different compositions.

The most significant compositional differences between the polytypes are that the I*a* chlorites lie along one extreme border of the II*b* compositional field and that the monoclinic I*b* chlorites lie well outside the same border. These specimens seem to have less tetrahedral Al than the other structural varieties, and the monoclinic I*b* types are especially Al-poor. The range of tetrahedral Al in the specimens studied is from 0.61 to 1.70 in 4.0 tetrahedral sites and the range in the Fe/Fe+Mg ratio is from 0.01 to 0.96. The average compositions of the specimens illustrated in Fig. 6 are given in the following chart.

Polytype	Number of specimens	Average tetrahedral Al	Average Fe/Fe+Mg
II*b*, β=97°	111	1.31	0.39
I*b*, β=90°	36	1.32	0.59
I*b*, β=97°	13	0.87	0.52
I*a*, β=97°	4	1.03	0.38

These compositions may be in error because of the possible effects on the *x*-ray spacings of cation ordering, of different pressures of formation, and of the presence of Fe^{3+} or other cations not included in the calibration standards. Until the compositions can be checked by direct chemical analysis, therefore, it is important to distinguish between the measurements involved and their interpretation. The measurement believed to be of most significance is that the I*b* structure based on a monoclinic-shaped cell has a layer thickness consistently larger than that of all other chlorites. This measurement is interpreted in terms of weaker interlayer bonds resulting from lesser tetrahedral substitution of Al for Si in the monoclinic-cell I*b* structure. The observed difference in average $c \sin \beta$ spacing of 0.14 Å between the I*b* and II*b* structures amounts to a difference of 0.44 atoms of tetrahedral Al according to Shirozu's spacing graph.

Tetrahedral cation composition can be especially effective in influencing the stability of a particular polytype. The amount of trivalent tetra-

hedral substitution determines both the amount of negative charge and the lateral dimensions of the tetrahedral sheets. These factors in turn influence the amount of electrostatic charge elsewhere in the structure and the degree of fit, and resultant distortion, of the component sheets. It can be shown, for example, that an ideal hexagonal tetrahedral sheet having a composition appropriate for the average II*b* chlorite is larger than the corresponding ideal octahedral sheet. The articulation of two tetrahedral sheets with one octahedral sheet to form the talc-like unit is accomplished only by distortion of the ideal geometry. The tetrahedral sheet is compressed laterally by rotation of the individual tetrahedra and by distortion of the ideal tetrahedral angles. The octahedral sheet is extended and thinned.

The monoclinic-cell I*b* structure was given an intermediate rating of 2 for its hydrogen bonding system in the chart at the beginning of this section. This rating is a result of an asymmetric arrangement of the tetrahedral rings in the initial and repeating talc sheets relative to the brucite sheet between. Opposing rings in the two talc sheets are so positioned that, if distorted according to the pattern determined in most layer silicates, minimum length hydrogen bonds are formed with hydroxyls on one side of the interleaved brucite sheet but much longer bonds with hydroxyls on the other side. The brucite sheet is under considerable strain in attempting to adjust to the effects of its asymmetric environment. A smaller amount of tetrahedral Al, as observed consistently for the monoclinic-cell I*b* polytype, would create a better fit between the ideal tetrahedral and octahedral sheets with less resulting distortion. Presumably the ideal composition for this structure is one that causes no resultant rotation of tetrahedra within the talc sheet. The brucite sheet then is not subjected to asymmetric distortion by the adjacent oxygen surfaces. The observations that the *x*-ray patterns of the I*b* specimens are diffuse and that the β angle is usually somewhat greater than the theoretical value of 97° probably indicate that the compositions are not quite ideal and that the brucite sheet is distorted asymmetrically to a certain extent. The orthohexagonal II*a* structure has a similar asymmetric arrangement of the talc and brucite sheets and, if observed, should fall in the same composition field.

Because the II*b* structure appears to represent the most stable, lowest energy configuration, reasons must be sought for the existence of the other chlorite layer types. The effect of screw dislocations and of different growth mechanisms probably can be neglected because we are concerned here with the layer types rather than their stacking sequences. Composition has already been mentioned as one possible factor that may modify polytype stability and abundance. Another factor to consider is the ex-

istence of equilibrium or non-equilibrium conditions, as related to the energy available in the environment of formation.

The stable chlorite in normal chlorite grade metamorphism and in medium and high temperature ore deposits is almost exclusively the II*b* form, suggesting that when sufficient energy is available the most stable polytype will form. Table 5 lists the occurrences of the three other polytypes recognized in this study. Many of these specimens occur in geologic environments or in mineral associations that suggest a lower temperature-pressure energy level than that for II*b* chlorite. This observation in turn suggests that the higher energy structures may have formed metastably under these conditions and that, given time or energy to do so, they would tend to invert to the stable II*b* structure. Field relationships indicate that the I*b* chlorites, in those occurrences where it can be studied, do recrystallize either to II*b* chlorite or to stilpnomelane during metamorphism. Von Engelhardt (1942) also has observed that the "chamositic" chlorites (orthohexagonal I*b*) contained in certain European oolitic iron ores tend to recrystallize to a monoclinic chlorite during metamorphism.

Those chlorites most apt to be considered diagenetic from their geologic associations are the orthohexagonal and monoclinic I*b* types. The oolitic iron-rich chlorites studied by von Engelhardt probably fall in this category, as do the orthohexagonal I*b* chlorites found filling the interstices in porous sandstones in the Pennsylvanian Fresnal group of New Mexico and in the Cretaceous Tuscaloosa sand of the Gulf Coast. Orthohexagonal I*b* chlorite occurs frequently in the Lake Superior iron-formations in areas of little or no metamorphism and is being studied in some detail in collaboration with S. A. Tyler and C. E. Dutton. The I*b* chlorite in some localities seems to have formed very early in the sedimentary history of the iron formation, along with greenalite and 7 Å chamosite, and in other localities seems to be a low-rank metamorphic mineral. One of the more convincing examples of a diagnetic occurrence is that of an iron-poor variety of I*b* chlorite replacing primary 1M muscovite granules (Tyler and Bailey, 1961) in an unmetamorphosed pyroclastic-bearing carbonate facies of the Gunflint iron-formation of Ontario. An iron-rich variety of I*b* chlorite replaces greenalite granules and in turn is replaced by stilpnomelane in low-rank metamorphism of a local silicate facies in the Pokegama quartzite of Minnesota. It is present in minor amounts replacing the type-greenalite of Leith (1903) in the Biwabic iron-formation of Minnesota and in more quantity in the interstices of the basal conglomerate of the Biwabic at the Embarrass mine. I*b* chlorite occurs in considerable quantity in the Riverton iron-formation at several mines near Florence, Wisconsin, and in massive metamorphic rocks associated

TABLE 5. Ia AND Ib CHLORITE SPECIMENS

Ib Chlorites (Orthohexagonal cell)

1. Chihuahua, Mexico. Green lenses in altered sill. UW 526-5599.
2. Keene-Antwerp district, New York. Quartz-chlorite-pyrite schist country rock to hematite ore body. UW 54-44-1.
3. Sacramento Mountains, New Mexico. Matrix in feldspathic sandstone near top of Fresnal group, upper Pennsylvanian. Donor: T. W. Oppel.
4. Tuscaloosa sandstone, upper Cretaceous, Gulf Coast area. Light green matrix to loosely cemented sand in core at 8300 feet. Donor: E. D. Glover and Socony Mobil Oil Company.
5. Ahmeek mine, Keweenaw Point, Michigan. Black coating in breccia with calcite, quartz, and Cu-arsenides. UW 53-104-7.
6. White Pine mine, Michigan. Greenish chlorite in veinlets in siltstone. Donor: R. H. Carpenter.
7. Amethyst Harbor, north shore of Lake Superior. Altered mafic minerals in coarse grained igneous rock. USGS 1664.
8. Presque Isle Park, Marquette, Michigan. Reworked periodotitic material in base of Eastern sandstone. Donor: S. A. Tyler.
9. Palmer area, Marquette district, Michigan. Late stage alteration of Negaunee iron-formation.
10. Ravenna-Pickett mine, Crystal Falls district, Michigan. Altered fragmental material, with 7 Å chamosite. Donor: S. A. Tyler.
11. Vicar mine, Gogebic district, Michigan. Vug fillings in Ironwood iron-formation, with pyrite and quartz. Donor: S. A. Tyler.
12. Thunder Bay, north shore of Lake Superior. Diagenetic replacement of 1M muscovite granules in tuffaceous, carbonate facies of upper Gunflint iron-formation. Donor: S. A. Tyler.
13. Stephen's mine, Mesabi district, Minnesota. Drill hole in upper Pokegama quartzite, in granules with quartz, greenalite, magnetite and stilpnomelane. Donor: S. A. Tyler.
14. Embarrass mine, Mesabi district, Minnesota. Matrix in basal conglomerate of Biwabic iron-formation. Donor: S. A. Tyler.
15. Florence, Wisconsin. Massive garnet-chlorite rock associated with iron-formation. USGS—Wis. Geol. Survey F6112.
16. Badger pit near Florence, Wisconsin. Interlayered with chert and hematite in Riverton iron-formation. USGS—Wis. Geol. Survey 1F101.
17. Davidson pit near Florence, Wisconsin. Slaty rock associated with Riverton iron-formation. USGS—Wis. Geol. Survey 1F102.
18. Florence, Wisconsin. Greenish layer, probably in Michigamme formation. Wis. Geol. Survey 12589.
19. Commonwealth mine, Florence, Wisconsin. Interlayered with chert and hematite in Riverton iron-formation. Donor: S. A. Tyler.
20. Florence mine near Florence, Wisconsin. Fracture filings in hematite ore body. USGS—Wis. Geol. Survey 1F100.

Ib chlorites (monoclinic cell)

1. New Britain, Connecticut. Vesicle fillings in basalt. UW 19408.
2. Hercules mine, Couer d'Alene, Idaho. Vein in Pb-Zn-Cu-Fe ore, with biotite and garnet. UW 59-16-12.

3. Hayange, France. Green-black matrix to oolites in black iron ore bed. Donor: E. D. Glover.

4. Moulaine, France. Green matrix to oolites in green iron ore bed. Donor: E. D. Glover.

5. White Pine mine, Michigan. Brownish chlorite replacing greenish orthohexagonal I*b* chlorite in veinlet in siltstone, with orthorhombic chalcocite and quartz. Donor: R. H. Carpenter.

6. Vicar mine, Michigan. Drill hole in altered pyroclastics of Ironwood iron-formation, with biotite and hematite. Donor: S. A. Tyler.

7. Vicar mine, Michigan. Granules associated with carbonate in the jasper-magnetite horizon of the Ironwood iron-formation. Donor: S. A. Tyler.

8. Near Mountain Iron, Mesabi district, Minnesota. Irregular granules in Upper Slaty Biwabic iron-formation. UW 45638.

9. Badger pit near Florence, Wisconsin. Massive olive-green material in Riverton iron-formation. USGS—Wis. Geol. Survey 1F101.

10. Silver Islet mine, Nipigon Bay. Altered mafic minerals in Keweenawan dike. USGS 1756.

11. Big Bay, north shore of Lake Superior. Altered mafic minerals in fine grained igneous rock. USGS 1519.

12. Portage Bay Island, north shore of Lake Superior. Altered mafic minerals in fine grained igneous rock. USGS 1569a.

13. Thunder Bay, north shore of Lake Superior. Altered mafic minerals in igneous rock. USGS 1670.

Ia chlorites

1. Erzincan district, Turkey. Purple Cr-chlorite in serpentinite-chromite complex. Donor: R. A. Bell.

2. Auburn mine, Mesabi district, Minnesota. From slickensided surface in upper part of Lower Slaty Biwabic iron-formation. Donor: S. A. Tyler.

3. Embarrass mine, Mesabi district, Minnesota. Recrystallization of earthy orthohexagonal I*b* chlorite near quartz veinlet in basal conglomerate of Biwabic iron-formation. Donor: S. A. Tyler.

4. Vicar mine, Gogebic district, Michigan. Drill hole in Ironwood iron-formation, interlayered with chert and stilpnomelane in the jasper-magnetite horizon. Donor: S. A. Tyler.

5. Londonderry, Western Australia. Cookeite in pegmatite. Donor: I. M. Threadgold.

6. Morning Star mine, Victoria, Australia. Cookeite in pegmatite. Donor: I. M. Threadgold.

7. Brazil. Cookeite in pegmatite. Donor: R. M. Thompson.

8. Mt. Mica, Paris, Maine. Cookeite in pegmatite. AMNH 13436.

9. Buckfield, Maine. Cookeite in pegmatite. AMNH 19452.

10. Haddam Neck, Connecticut. Cookeite in pegmatite. AMNH 13440.

---

with the iron-formation. It is found in the Ravenna-Pickett mine in the Crystal Falls district of Michigan, along with 7 Å chamosite, in the alteration products of fragmental material, probably pyroclastic in origin. In the Palmer district of Michigan I*b* chlorite occurs in veins and openings where II*b* chlorite in the Negaunee iron-formation seems to have undergone a late stage retrograde alteration.

We have found the monoclinic I*b* chlorite in two French oolitic iron ores from Hayange and Moulaine. In the Lake Superior iron-formations monoclinic I*b* chlorite is often associated closely with the orthohexagonal I*b* variety. It has been recognized in irregular granules in the Upper Slaty Biwabic iron-formation of Minnesota, in altered pyroclastics and in layers within the Ironwood iron-formation in the Gogebic district of Michigan, and in layers within the Riverton iron-formation of Wisconsin. We have no definite evidence as to whether there is any preference for the monoclinic or orthohexagonal I*b* structure to form first in a given low energy environment. One might predict on theoretical grounds that the higher energy monoclinic I*b* structure should be favored in a metastable crystallization. It should be easier also to satisfy the smaller tetrahedral Al substitution required for the monoclinic I*b* structure. Thin section study shows that in some specimens the I*b* chlorites replace pre-existing layer silicates, such as 1M muscovite, greenalite, or 7 Å chamosite, in various stages of diagenesis or low-rank metamorphism. We have no definite evidence to indicate that this is always true, but it is interesting to notice the comparison with the synthesis studies of Nelson and Roy (1958) in which Mg-chlorites were found to be preceded at low temperatures, perhaps metastably, by 7 Å structures of similar composition.

Despite the evidence that some specimens of orthohexagonal- and monoclinic-cell I*b* chlorite may form diagenetically, it is evident from the occurrences listed in Table 5 that these polytypes also can form over a considerable range of environmental conditions. In some, but not all, specimens increasing iron and tetrahedral Al content seems to be correlated with increasing temperature of formation. Included in this category would be the monoclinic-cell I*b* chlorite associated with biotite and garnet in veins in Pb-Zn-Cu-Fe ore of the Couer d'Alene district, Idaho, and the orthohexagonal I*b* chlorites from hydrothermal copper-quartz veins described by Shirozu (1958a, 1960a). It is not clear at this stage why the II*b* structure should not have formed under these relatively high energy conditions.

The I*a* chlorite is believed to be stable at slightly higher temperatures than for the orthohexagonal I*b* chlorite. Evidence for this belief is found in the recrystallization of an earthy I*b* type to thin flakes of I*a* chlorite in a selvage around a small quartz veinlet at the Embarrass mine in Minnesota. The only composition change evident by the *x*-ray spacing technique is a slight decrease in tetrahedral Al upon recrystallization. At the Vicar mine in Michigan I*a* chlorite exists interlayered with stilpnomelane in low-rank metamorphism of the Ironwood iron-formation. Elsewhere the orthohexagonal I*b* chloride was found to be replaced by stilpnomelane in metamorphism, a further indirect evidence for the relative stabilities of the I*a* and I*b* types. The Erzincan I*a* Cr-chlorite

associated with a chromite-serpentine rock is probably hydrothermal. The cookeites are all pegmatitic, probably associated with late alteration phases.

The evidence suggesting a higher temperature of formation for I*a* chlorite than for orthohexagonal I*b* chlorite is contrary to the prediction of relative stabilities based on cation repulsion and hydrogen bond length ratings. The stability relations may result from modification of these ratings by the particular compositions involved, Li-Al in cookeite, ordered Cr and Al sites in the Erzincan chlorite, and low tetrahedral-Al plus high talc-Fe in the three Mg-Fe chlorites examined. These compositions may alleviate the high Coulomb energy due to cation repulsion by affording an unusually good hydrogen bond system.

The interpretations presented here as to the influence of structure, composition, and environment on chlorite polytype stabilities are necessarily tentative. Detailed structure determinations now in progress undoubtedly will clarify the influence of structure upon polytype stability. It is hoped to combine this sort of information with further *x*-ray and petrographic studies of specimens for which close compositional and environmental control can be obtained.

Acknowledgments

This study was supported in part by the Research Committee of the Graduate School from funds supplied by the Wisconsin Alumni Research Foundation. We are indebted to Dr. Brian Mason of the American Museum of Natural History, Dr. R. M. Thompson of the University of British Columbia, Dr. H. Shirozu of Kyushu University, Dr. C. E.Dutton of the U. S. Geological Survey, Dr. R. A. Bell of McPhar Geophysics, Ltd., E. D. Glover of Socony Mobil Oil Research Laboratory, Dr. S. A. Tyler, Dr. E. N. Cameron, and Dr. R. C. Emmons, as well as a number of students, at the University of Wisconsin for the loan or donation of chlorite specimens. Some of the *x*-ray photographs were taken by Miss Judy Smith and R. A. Eggleton. Computations were carried out in the Numerical Analysis Laboratory of the University of Wisconsin.

References

Bailey, S. W. and S. A. Tyler (1960), Clay minerals associated with the Lake Superior iron ores. *Econ. Geol.*, **55**, 150–175.

Brammall, A., J. G. C. Leech and F. A. Bannister (1937), The paragenesis of cookeite and hydromuscovite associated with gold at Ogofau, Carmarthenshire. *Mineral. Mag.*, **24**, 507–521.

Brindley, G. W. (1951), The crystal structure of some chamosite minerals. *Mineral. Mag.*, **29**, 502–525.

———, Beryl M. Oughton, and K. Robinson (1950), Polymorphism of the chlorites. I. Ordered structures. *Acta Cryst.*, **3**, 408–416.

BROWN, B. E. AND S. W. BAILEY (1960), Crystal structure of a chromium chlorite (abst.). *Geol. Soc. Amer. Bull.*, **71,** 1835.

GARRIDO, J. (1949), Structure cristalline d'une chlorite chromifere. *Bull. Soc. Franc. Miner. Crist.*, **72,** 549–570.

GILLERY, F. H. (1959), The X-ray study of synthetic Mg-Al serpentines and chlorites. *Am. Mineral.*, **44,** 143–152.

HOWELLS, E. R., D. C. PHILLIPS, AND D. ROGERS (1950), The probability distribution of X-ray intensities. II. Experimental investigation and the X-ray detection of centres of symmetry. *Acta Cryst.*, **3,** 210–214.

LAPHAM, D. M. (1958), Structural and chemical variation in chromium chlorite. *Am. Mineral.*, **43,** 921–956.

LEITH, C. K. (1903), The Mesabi iron-bearing district of Minnesota. *U. S. Geol. Survey Mono.*, **43,**

MATHIESON, A. McL. (1958), Mg-vermiculite: A refinement and re-examination of the crystal structure of the 14.36 Å phase. *Am. Mineral.*, **43,** 216–277.

——— AND G. F. WALKER (1954), Crystal structure of magnesium-vermiculite. *Am. Mineral.*, **39,** 231–255.

MCMURCHY, R. C. (1934), The crystal structure of the chlorite minerals. *Zeit. Krist.*, **88,** 420–432.

NELSON, B. W., AND R. ROY (1958) , Synthesis of the chlorites and their structural and chemical constitution. *Am. Mineral.*, **43,** 707–725.

NEWHAM, R. E. (1961), A refinement of the dickite structure and some remarks on polymorphism in kaolin minerals. *Mineral. Mag.*, **32,** 683–704.

PAULING, L. (1930), The structure of the chlorites. *Proc. Nat. Acad. Sci.*, **16,** 578–582.

RADOSLOVICH, E. W. (1960), The structure of muscovite, $KAl_2(Si_3Al)O_{10}(OH)_2$. *Acta Cryst.*, **13,** 919–932.

ROBINSON, K. AND G. W. BRINDLEY (1949), A note on the crystal structure of the chlorite minerals. *Proc. Leeds Phil. Soc.*, **5,** 102–108.

SHIROZU, H., (1955), Iron-rich chlorite from Shogasé, Kochi Prefecture, Japan. *Mineral. Jour. (Japan)*, **1,** 224–232.

——— (1958a), *X*-ray powder patterns and cell dimensions of some chlorites in Japan, with a note on their interference colors. *Mineral. Jour. (Japan)*, **2,** 209–223.

——— (1958b), Aluminian serpentine and associated chlorite from Usagiyama, Fukuoka Prefecture, Japan. *Mineral. Jour. (Japan)*, **2,** 298–310.

——— (1960a), Ionic substitution in iron-magnesium chlorites. *Mem. Faculty Sci., Kyushu Univ., D, Geol.*, **9,** 183–186.

——— (1960b), Determination of the chemical composition of chlorites by the *X*-ray and optical methods (in Japanese). *Jour. Japan. Assoc. Miner. Petr. Econ. Geol.*, **44,** 18–22.

STEINFINK, H. (1958a), The crystal structure of chlorite. I. A monoclinic polymorph. *Acta Cryst.*, **11,** 191–195.

——— (1958b), The crystal structure of chlorite. II. A triclinic polymorph. *Acta Cryst.*, **11,** 195–198.

——— (1961), Accuracy in structure analysis of layer silicates: Some further comments on the structure of prochlorite. *Acta Cryst.*, **14,** 198–199.

——— AND G. BRUNTON (1956), The crystal structure of amesite. *Acta Cryst.*, **9,** 487–492.

TYLER, S. A., AND S. W. BAILEY (1961), Secondary glauconite in the Biwabic iron-formation of Minnesota. *Econ. Geol.*, **56,** 1033–1044.

VON ENGELHARDT, W. (1942), Die Strukturen von Thuringit, Bavalit und Chamosit und ihre Stellung in der Chloritgruppe. *Zeit. Krist.*, **104,** 142–159.

Manuscript received, January 3, 1962.